

Vortex modes supported by spin-orbit coupling in a laser with saturable absorption

Thawatchai Maytevarunyoo¹, Boris A. Malomed^{2,3}, Dmitry V. Skryabin⁴

¹*Department of Electrical and Computer Engineering,*

Faculty of Engineering Naresuan University, Phitsanulok 65000, Thailand

²*Department of Physical Electronics, School of Electrical Engineering, Faculty of Engineering, and Center for Light-Matter Interaction, Tel Aviv University, Tel Aviv 69978, Israel*

³*ITMO University, St. Petersburg 197101, Russia and*

⁴*Department of Physics, University of Bath, Bath, BA2 7AY, UK*

We introduce a system of two component two-dimensional (2D) complex Ginzburg-Landau equations (CGLEs) with spin-orbit-coupling (SOC) describing a wide-aperture microcavity laser with saturable gain and absorption. We report families of two-component self-trapped dissipative laser solitons in this system. The SOC terms are represented by the second-order differential operators, which sets the difference, $|\Delta S| = 2$, between the vorticities of the two components. We have found stable solitons of two types: vortex-antivortex (VAV) and semi-vortex (SV) bound states, featuring vorticities $(-1, +1)$ and $(0, 2)$, respectively. In previous works, 2D localized states of these types were found only in models including a trapping potential, while we are dealing with the self-trapping effect in the laterally unconfined (free-space) model. The SV states are stable in a narrow interval of values of the gain coefficients. The stability interval is broader for VAV states, and it may be expanded by making SOC stronger (although the system without SOC features a stability interval too). We have found three branches of stationary solutions of both VAV and SV types, two unstable and one stable. The latter one is an attractor, as the unstable states spontaneously transform into the stable one, while retaining vorticities of their components. Unlike previously known 2D localized states, maintained by the combination of the trapping potential and SOC, in the present system the VAV and SV complexes are stable in the absence of diffusion. In contrast with the bright solitons in conservative models, chemical potentials of the dissipative solitons reported here are positive.

I. INTRODUCTION

The spin-orbit coupling (SOC), which was originally predicted in the form of the Dresselhaus [1] and Rashba [2, 3] Hamiltonians, is a fundamentally important effect in physics of semiconductors [4–6]. More recently, much interest was drawn to the possibility to emulate the SOC phenomenology, in its “clean” form, in spinor (two-component) atomic Bose-Einstein condensates (BECs), by creating settings whose Hamiltonians can be mapped into the Dresselhaus and Rashba forms (or a combination of both) [7–9], see also reviews [10–12]. In these contexts, adequate mean-field SOC models are provided by systems of nonlinear Gross-Pitaevskii equations (GPEs) coupled by linear-mixing terms composed of first-order spatial derivatives.

Parallel to these developments, SOC effects were realized in the exciton-polariton fields populating semiconductor microcavities operating in the strong coupling regime [13]–[17], and in many other optical systems [18], which are, however, less relevant in the present context. It is important to note that SOC in polaritonic microcavities can have two different physical origins, *viz.*, due to the underlying SOC between excitons, or between the photonic modes. Thus, the existence of polaritons is not required to observe SOC, and therefore the microcavities operating in the regime of weak coupling between light and matter, when polaritons are not formed, can be used to realize SOC effects. Below we make use of this opportunity, considering a planar microcavity that includes ingredients providing both saturable gain and absorption [20, 25, 26]. This configuration is well known for its ability to maintain mode-locking of transverse modes, leading to the formation of bright spatial solitons, as well as to provide interplay of transverse and longitudinal modes leading to 3D effects, see, e.g., Refs. [22]–[27]. However, SOC effects have not been so far purposefully studied in these settings. In microcavities, the SOC originates from the splitting of resonances of the linearly (in-plane) polarized modes, whose dominant electric-field components are perpendicular (TE) and parallel (TM) to the in-plane component of the carrier wave vector. Writing the field equations in terms of circular polarizations produces the SOC terms with the second-order derivatives in Eqs. (1) and (2), see below, which were previously discussed in detail, see, e.g., [19]. Note that for transversely inhomogeneous states (in particular, self-trapped solitons) the SOC terms are going to be important even for states with the zero in-plane momentum.

A theoretical analysis of systems combining the cubic attractive interactions of the BEC wave functions and linear spatial-derivative SOC in two dimensions (2D) has revealed unexpected results. First, in the absence of a trapping potential, SOC represented by the Rashba Hamiltonian produces two species of *stable* 2D solitons. These are *semi-vortices* (SVs, alias *half-vortices* [28]) with one zero-vorticity component, and the other one carrying vorticity $S = \pm 1$, and *mixed modes* (MMs), so called because they mix zero-vorticity terms and ones with $S = \pm 1$ in both components [29–31]. These results are drastically different from the well-known ones obtained for traditional GPE models in 2D,

which produce *Townes solitons* with zero vorticity [32], and their ring-shaped vorticity-carrying extensions [33]–[36]. The instability of the Townes solitons is driven by the *critical collapse* in the 2D space with the cubic attraction [37, 38], while the vortex-ring solitons are subject to a still stronger ring-splitting instability [39, 40]. The presence of the SOC terms changes the situation, as they bring a coefficient which fixes a length scale in the system, which, in turn, breaks the scaling invariance that makes norms of the Townes’ solitons degenerate (the entire family of these solitons has a single value of the norm). The lifting of the norm degeneracy pushes it below the degenerate value, which determines the collapse-onset threshold, hence the collapse cannot occur anymore. This mechanism secures the stabilization of both the SVs and MMs, and lends them the role of the otherwise missing ground states [30, 31].

A difference introduced by the microcavity SOC terms is their second-order derivatives, giving rise to the vorticity difference between two spin (circularly polarized) components to be $|\Delta S| = 2$, rather than $|\Delta S| = 1$ as in the above-mentioned models of atomic BEC. In particular, the analysis of the composite modes in the exciton-polariton system, which includes a harmonic-oscillator trapping potential, was recently elaborated in Ref. [41]. An essential result was the identification of stability regions for MMs and vortex-antivortex (VAV) complexes, with vorticities $S = \pm 1$ in the two components (thus complying with the above-mentioned constraint, $\Delta S = 2$). An area of the MM-VAV bistability was identified too, and stable SVs were found when the Zeeman splitting was added to the two-component system.

While trapping potentials are an important ingredient in various systems, see, e.g., [42, 43] in addition to the above, it is also relevant to construct stable composite modes supported by SOC in the laterally unbound settings. In particular, laser systems with and without saturable absorbers [20, 21, 25–27] are known to support self-bound vortex rings [21, 27]. A possible practical realisation of a laser model considered below is a wide-aperture semiconductor laser with a saturable absorber section similar to the ones used in [20, 25, 26], where the SOC effects originate from the above mentioned TE-TM splitting of the cavity resonances. Theoretically, but without the SOC effects, the model used below was elaborated in a series of papers by Rosanov and co-authors, see, e.g., [44–46], and references there in. We generalise the Rosanov’s approach by including the SOC terms represented by second derivatives mixing the two spin components. The system may also include effects of diffusion, but, unlike the setting explored in Ref. [41] and in many other models [48]–[50], the presence of the diffusion is not necessary for the stability of 2D states in the present case. Below, we identify two species of stable self-bound vortex modes, *viz.*, VAVs and SVs, both built of components obeying the constraint of $\Delta S = 2$. In particular, the VAVs feature two mutually symmetric components with vorticities $S = \pm 1$, while the amplitude of the SV’s zero-vorticity component is much larger than the amplitude of its vortical counterpart.

It is relevant to mention that VAVs are quite similar to two-component states, produced by systems of 2D [51–53] and 3D [54] nonlinearly-coupled GPEs, with opposite vorticities, $\pm S$, and identical density profiles in the components. In the latter context, the bound states of this type were called “hidden-vorticity modes”, as, on the contrary to their counterparts with equal vorticities in both components, the total angular momentum of the hidden-vorticity states is zero. In addition to that, conservative systems with the nonlinear (cross-phase-modulation) interaction between two components (and no linear coupling between them) maintain bound states similar to SVs, with zero and nonzero vorticities in the components [55, 56].

The subsequent presentation is organized as follows. The system of complex Ginzburg-Landau equations (CGLEs) with the saturable gain, coupled by the SOC terms, is introduced in Section II. The same section also reports some simple analytical results (necessary conditions for the existence of stable 2D dissipative solitons). Numerical results, produced by the systematic investigation of the 2D system, are reported in Section III, for two above-mentioned species of stable modes, *viz.*, VAVs and MMs. The paper is concluded by Section IV.

II. THE MODEL AND ANALYTICAL ESTIMATES

In terms of scaled time t and coordinates (x, y) , the system of CGLEs for wave functions ψ_{\pm} of the two spin components, with the linear loss, whose coefficient is scaled to be 1, saturable gain and saturable absorption, which are represented, respectively, by coefficients $g > 0$ and $a > 0$, and SOC linear mixing with real coefficient β , is written as

$$i\partial_t\psi_+ = -(1 - i\eta)(\partial_x^2 + \partial_y^2)\psi_+ + if\psi_+ + \beta(\partial_x - i\partial_y)^2\psi_-, \quad (1)$$

$$i\partial_t\psi_- = -(1 - i\eta)(\partial_x^2 + \partial_y^2)\psi_- + if\psi_- + \beta(\partial_x + i\partial_y)^2\psi_+, \quad (2)$$

$$f = -1 + \frac{g}{1 + \varepsilon(|\psi_+|^2 + |\psi_-|^2)} - \frac{a}{1 + (|\psi_+|^2 + |\psi_-|^2)}. \quad (3)$$

Here, the coefficient in front of the Laplacian, which represents the diffraction, is also scaled to be 1 (in this notation, physically relevant values of the SOC coefficient, $|\beta|$, are definitely smaller than 1), and positive $\varepsilon < 1$ defines a

relative saturation strength of the gain and absorption. The dispersive component of the linear loss (diffusion) may be present, with coefficient $\eta > 0$, but, in fact, the inclusion of this term, whose physical origin may not be obvious, is not necessary for producing stable 2D modes, therefore we set $\eta = 0$ in what follows below. The generic situation may be adequately represented by parameters

$$\varepsilon = 0.1, \quad a = 2, \quad (4)$$

which implies weak saturation of the gain in comparison with absorption, while the gain and SOC strengths, g and β , will be varied as physically relevant parameters controlling modes generated by the system. Stationary states with real chemical potential μ are sought as

$$\psi_{\pm} = e^{-i\mu t} u_{\pm}(x, y), \quad (5)$$

where complex stationary wave functions u_{\pm} obey the following equations:

$$\mu u_{+} = -(1 - i\eta)(\partial_x^2 + \partial_y^2)u_{+} + iF(x, y)u_{+} + \beta(\partial_x - i\partial_y)^2 u_{-}, \quad (6)$$

$$\mu u_{-} = -(1 - i\eta)(\partial_x^2 + \partial_y^2)u_{-} + iF(x, y)u_{-} + \beta(\partial_x + i\partial_y)^2 u_{+}, \quad (7)$$

$$F(x, y) \equiv -1 + \frac{g}{1 + \varepsilon(|u_{+}|^2 + |u_{-}|^2)} - \frac{a}{1 + (|u_{+}|^2 + |u_{-}|^2)}. \quad (8)$$

For the analysis of stability of stationary states, we define perturbed solutions as

$$\psi_{\pm}(x, y, t) = e^{-i\mu t} \left\{ u_{\pm}(x, y) + \delta \left[v_{\pm}(x, y) e^{\lambda t} + w_{\pm}^{*}(x, y) e^{\lambda^{*} t} \right] \right\}, \quad (9)$$

where δ is a real infinitesimal amplitude of the perturbations, λ is a complex eigenvalue, and complex perturbation eigenmodes, $v_{\pm}(x, y)$ and $w_{\pm}(x, y)$, satisfy the linearized equations

$$(\mu + i\lambda)v_{+} = -(1 - i\eta)(\partial_x^2 + \partial_y^2)v_{+} + \beta(\partial_x - i\partial_y)^2 v_{-} + iF(x, y)v_{+} + iu_{+} [G(x, y)(u_{+}^{*}v_{+} + u_{+}w_{+} + u_{-}^{*}v_{-} + u_{-}w_{-})], \quad (10)$$

$$(\mu + i\lambda)v_{-} = -(1 - i\eta)(\partial_x^2 + \partial_y^2)v_{-} + \beta(\partial_x + i\partial_y)^2 v_{+} + iF(x, y)v_{-} + iu_{-} [G(x, y)(u_{+}^{*}v_{+} + u_{+}w_{+} + u_{-}^{*}v_{-} + u_{-}w_{-})], \quad (11)$$

$$(\mu - i\lambda)w_{+} = -(1 + i\eta)(\partial_x^2 + \partial_y^2)w_{+} + \beta(\partial_x + i\partial_y)^2 w_{-} - iF(x, y)w_{+} - iu_{+}^{*} [G(x, y)(u_{+}w_{+} + u_{+}^{*}v_{+} + u_{-}w_{-} + u_{-}^{*}v_{-})], \quad (12)$$

$$(\mu - i\lambda)w_{-} = -(1 + i\eta)(\partial_x^2 + \partial_y^2)w_{-} + \beta(\partial_x - i\partial_y)^2 w_{+} - iF(x, y)w_{-} - iu_{-}^{*} [G(x, y)(u_{+}w_{+} + u_{+}^{*}v_{+} + u_{-}w_{-} + u_{-}^{*}v_{-})], \quad (13)$$

where we have defined a real function,

$$G(x, y) \equiv \frac{a}{(1 + |u_{+}|^2 + |u_{-}|^2)^2} - \frac{\varepsilon g}{(1 + \varepsilon(|u_{+}|^2 + |u_{-}|^2))^2}. \quad (14)$$

As usual, the stability condition is $\text{Re}(\lambda) \leq 0$ for all eigenvalues.

The system of equations (10)-(13) can be written as an eigenvalue problem in the matrix form:

$$i\mathbf{L}\Psi = \lambda\Psi \quad (15)$$

where

$$\mathbf{L} = \begin{pmatrix} \mathbf{L}_{11} & \mathbf{L}_{12} & \mathbf{L}_{13} & \mathbf{L}_{14} \\ \mathbf{L}_{21} & \mathbf{L}_{22} & \mathbf{L}_{23} & \mathbf{L}_{24} \\ \mathbf{L}_{31} & \mathbf{L}_{32} & \mathbf{L}_{33} & \mathbf{L}_{34} \\ \mathbf{L}_{41} & \mathbf{L}_{42} & \mathbf{L}_{43} & \mathbf{L}_{44} \end{pmatrix}, \quad \Psi = \begin{pmatrix} v_{+} \\ v_{-} \\ w_{+} \\ w_{-} \end{pmatrix} \quad (16)$$

$$\mathbf{L}_{11,22} \equiv (1 - i\eta) (\partial_x^2 + \partial_y^2) - iF(x, y) - iu_{+,-} \left[G(x, y) \left(u_{+/-}^* \right) \right] + \mu, \quad (17)$$

$$\mathbf{L}_{12,21} \equiv -\beta(\partial_x - / + i\partial_y)^2 - iu_{+,-} \left[G(x, y) \left(u_{-/+}^* \right) \right], \quad (18)$$

$$\mathbf{L}_{13,14} \equiv -iu_+ [G(x, y) (u_{+,-})], \mathbf{L}_{23,24} \equiv -iu_- [G(x, y) (u_{+,-})], \quad (19)$$

$$\mathbf{L}_{31,32} \equiv -iu_+^* [G(x, y) (u_{+,-}^*)], \mathbf{L}_{41,42} \equiv -iu_-^* [G(x, y) (u_{+,-}^*)], \quad (20)$$

$$\mathbf{L}_{33,44} \equiv -(1 + i\eta) (\partial_x^2 + \partial_y^2) - iF(x, y) - iu_{+,-}^* [G(x, y) (u_{+/-})] - \mu, \quad (21)$$

$$\mathbf{L}_{34,43} \equiv \beta(\partial_x +, -i\partial_y)^2 - iu_{+,-}^* [G(x, y) (u_{-,+})]. \quad (22)$$

The spectrum of the linear-stability operator \mathbf{L} was constructed by means of the Fourier collocation method.

To complete the formulation of the stability-analysis framework, we notice that, being interested in stable dissipative solitons, a necessary condition is the stability of the zero background in Eqs. (1), (2) and (3), which obviously amounts to condition $g < 1 + a$. On the other hand, a necessary condition for the ability of the saturable gain to maintain nontrivial modes is that the largest value of $f(n \equiv |\psi_+|^2 + |\psi_-|^2)$ in Eq. (3), which is attained at density

$$n_0 = \frac{\sqrt{a} - \sqrt{\varepsilon g}}{\sqrt{\varepsilon} (\sqrt{g} - \sqrt{\varepsilon a})}, \quad (23)$$

must be positive. The substitution of n_0 in Eq. (3) yields a lower bound for g , which, if combined with the above-mentioned upper one, $g < 1 + a$, defines the interval in which the gain coefficient may take its values:

$$\sqrt{\varepsilon a} + \sqrt{1 - \varepsilon} < g < 1 + a \quad (24)$$

[the compatibility condition for a and ε , following from Eq. (23), $\sqrt{\varepsilon a} + \sqrt{1 - \varepsilon} < 1 + a$, always holds]. An additional restriction on g is imposed by the condition that expression (23) must be positive too:

$$\varepsilon a < g < a/\varepsilon. \quad (25)$$

Note that for values $a = 2$ and $\varepsilon = 0.1$ adopted here, interval (24) amounts to

$$1.396 < g < 3, \quad (26)$$

while interval (25) is much broader and may therefore be disregarded.

Our objective is to construct solutions of the CGLE system of Eqs. (1) and (2) in the form of 2D bright solitons morphed as bound states of two components with certain values of integer vorticities, $m - 1$ and $m + 1$, so that they comply with the above-mentioned constraint, $\Delta S = 2$. In polar coordinates (r, θ) , the relevant solutions with real chemical potential μ can be defined as

$$\psi_+ = \phi_+(r) \exp[-i\mu t + i(m - 1)\theta], \quad \psi_- = \phi_-(r) \exp[-i\mu t + i(m + 1)\theta], \quad (27)$$

with complex amplitude functions $\phi_{\pm}(r)$ satisfying the radial equations:

$$\begin{aligned} \mu\phi_+ &= -(1 - i\eta) \left[\frac{d^2}{dr^2} + \frac{1}{r} \frac{d}{dr} - \frac{1}{r^2} (m - 1)^2 \right] \phi_+ \\ &+ if\phi_- + \beta \left(\frac{d^2}{dr^2} + \frac{2m + 1}{r} \frac{d}{dr} + \frac{m^2 - 1}{r^2} \right) \phi_-, \\ \mu\phi_- &= -(1 - i\eta) \left[\frac{d^2}{dr^2} + \frac{1}{r} \frac{d}{dr} - \frac{1}{r^2} (m + 1)^2 \right] \phi_- \\ &+ if\phi_+ + \beta \left(\frac{d^2}{dr^2} - \frac{2m - 1}{r} \frac{d}{dr} + \frac{m^2 - 1}{r^2} \right) \phi_+, \end{aligned} \quad (28)$$

where f is defined by Eq. (3), with $|\psi_{\pm}|$ replaced by $|\phi_{\pm}|$.

The boundary condition for Eq. (28) at $r \rightarrow 0$ is that ϕ_{\pm} must be vanishing as $r^{|m \mp 1|}$ at $r \rightarrow 0$, except for the case of $m \mp 1 = 0$, when the boundary condition is $d\phi_{\pm}/dr|_{r=0} = 0$. At $r \rightarrow \infty$, soliton solutions must feature the exponential decay,

$$\phi_{\pm}(r) \sim r^{-1/2} \exp(-(\lambda_r + i\lambda_i)r), \quad (29)$$

with $\lambda_r > 0$ and, generally, a nonvanishing imaginary part of the decay rate, λ_i . The substitution of asymptotic expression (29) in Eq. (28) and the linearization for the exponentially small amplitude functions leads to the relation between the imaginary and real parts,

$$\lambda_i = -\frac{1+a-g}{2(1 \pm \beta)\lambda_r}, \quad (30)$$

and a quadratic equation for λ_r^2 ,

$$4(1 \pm \beta)^2 (\lambda_r^2)^2 + 4(1 \pm \beta)\mu (\lambda_r^2) - (1+a-g)^2 = 0, \quad (31)$$

a larger root of which yields a relevant value, $\lambda_r^2 > 0$ (here, sign \pm is unrelated to the subscript of ϕ_{\pm}). An essential consequence of Eq. (31) is that, while in the conservative model, in which the linear-loss factor, $(1+a-g)$, does not appear, $\lambda_r^2 > 0$ is only possible for a negative chemical potential, $\mu < 0$ (at least, in the physically relevant case of $|\beta| < 1$), in the dissipative system $\mu > 0$ is admitted too. Indeed, all the numerical solutions, reported below, have been obtained with $\mu > 0$. Further, it should be stressed that, as in the case of generic dissipative solitons [57]-[59], relevant solutions exist only at isolated (positive) eigenvalues of μ . The solitons are characterized by the total integral power (norm),

$$N = \int \int \left[|\psi_+(x, y)|^2 + |\psi_-(x, y)|^2 \right] dx dy \equiv 2\pi \int_0^\infty \left[|\phi_+(r)|^2 + |\phi_-(r)|^2 \right] r dr, \quad (32)$$

The analysis is carried out below for two most essential species of the soliton complexes, *viz.*, VAVs corresponding to $m = 0$ (so called because their components carry opposite vorticities, -1 and $+1$), and SVs, corresponding to $m = 1$, with component vorticities 0 and 2 . For $m \geq 2$, bound states (27) resemble “excited states” of SVs, introduced in the model of the atomic BEC in Ref. [29], and, as well as in that setting, it is plausible that they are completely unstable.

III. NUMERICAL RESULTS

Numerical solutions for the soliton modes were obtained by splitting complex functions $\phi_{\pm}(r) \exp[i(m \mp 1)\theta]$, defined in Eq. (27), into real and imaginary parts, and solving the resultant equations in the Cartesian coordinates by means of the modified squared-operator method [60]. The respective eigenvalues μ were found simultaneously with the stationary modes. Stability of the stationary states was identified by means of systematic direct simulations of perturbed evolution of the stationary states, governed by Eqs. (1) and (2), and, in parallel, by calculating the stability eigenvalues, as determined by Eqs. (15) and (16).

A. Vortex-antivortex (VAV) complexes, $m = 0$

VAV modes, with $m = 0$, were constructed as solutions of the stationary equations, starting with the input adjusted to vorticities ± 1 in the two components,

$$\phi_+(r) = \phi_-(r) = \phi_0 r \exp(-\alpha r^2), \quad (33)$$

with some empirically chosen real parameters ϕ_0 and α , a typical value being $\alpha = 0.05$. As said above, parameters $\eta = 0$, $a = 2$, $\varepsilon = 0.1$, were fixed in Eqs. (1), (2) and (28), while the SOC and gain strengths β and g were varied. As a result, three coexisting VAV families were found, two unstable and one stable. Figure 1 represents them by showing their integral power (32) and the peak density,

$$n_{\max} \equiv \max \left\{ |\psi_+(x, y)|^2 + |\psi_-(x, y)|^2 \right\}, \quad (34)$$

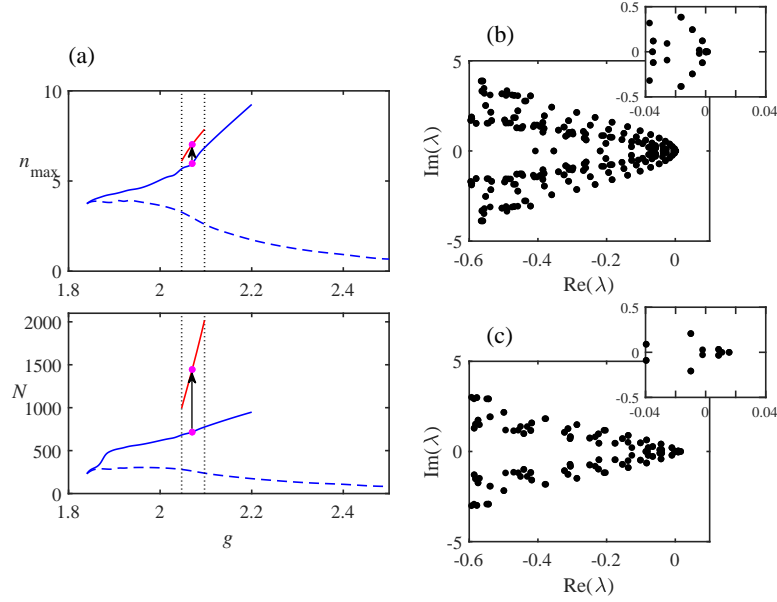


FIG. 1: (a) The peak density (top), defined as per Eq. (34), and the integral power (norm), defined as per Eq. (32), of VAV (vortex-antivortex) modes vs. the gain coefficient, g , at the fixed SOC coefficient, $\beta = 0.1$, with other parameters fixed as in Eq. (4). The solid and dashed blue lines represent two unstable families, and the red segment designates the stable one, in the stability window (36), marked by vertical dashed lines. (b) The spectrum for the stable stationary VAV at $g = 2.070$, which is marked by the magenta dot belonging to the red branch in (a). (c) The spectrum for the unstable VAV found at $g = 2.070$, which is marked by the magenta dot belonging to the blue branch in (a). In panel (b) and (c), insets zoom the vicinity of $\lambda = 0$.

vs. g , at fixed $\beta = 0.1$. In particular, the pair of unstable branches (continuous and dashed blue lines in Fig. 1) emerge from a bifurcation point at

$$g \approx 1.84. \quad (35)$$

The stable (red) branch is shown only in the relatively narrow window where it remains stable,

$$2.047 < g < 2.097, \quad (36)$$

which is bounded by vertical dashed lines in Fig. 1. Note that, although being much more narrow than interval (24) determined by the above-mentioned necessary conditions, stability region (36) is located quite close to the center of the broad interval (24). It is relevant to note that, the narrow interval (36), and similar intervals reported below, can be realized in terms of actual physical parameters of laser cavities with the saturable gain and loss, as it follows from Refs. [21, 25–27].

As concerns the chemical potential of the stable branch, in the stability interval (36) it decreases nearly linearly, as a function of g , from $\mu(g = 2.047) = 0.127$ to $\mu(g = 2.097) = 0.081$. We stress that, as mentioned above, these values are positive, on the contrary to necessarily negative chemical potential for solitons in conservative models. As for the two unstable branches, they produce positive and almost constant μ in the same interval (36).

At $g < 2.047$, the development of the instability of the branches shown by the blue lines in Fig. 1 leads to their decay towards the zero solution, while at $g > 2.097$ the amplitude features exponential growth (blowup, see Fig. 4). Inside stability interval (36), the stable branch (the red segment in Fig. 1) is an *attractor*: solitons belonging to either unstable branch spontaneously transform into ones belonging to the stable branch, as shown in Fig. 2. The outcome of the transformation is identical to the VAV mode that may be found as the stationary solution, see an example in Fig. 3. We did not aim to extend the red branch in Fig. 1 into the areas where it is unstable, i.e., $g < 2.047$ and $g > 2.097$, see Eq. (36).

As concerns (in)stability eigenvalues, produced by the linearized equations (15) and (16), typical examples of stable and unstable spectra are displayed in Figs. 2(b), 3(b), 4(b) and 7(b), respectively. These results are consistent with the conclusions made on the basis of systematic direct simulations of the perturbed evolution of the VAV modes.

The results of the investigation of the VAV modes are summarized in Fig. 5, which displays the stability region in the plane of the varying parameters, g and β (the gain and SOC strengths). It is worthy to note that the instability proceeds via the decay or blowup, without breaking the axial symmetry of the VAVs. This is a drastic difference

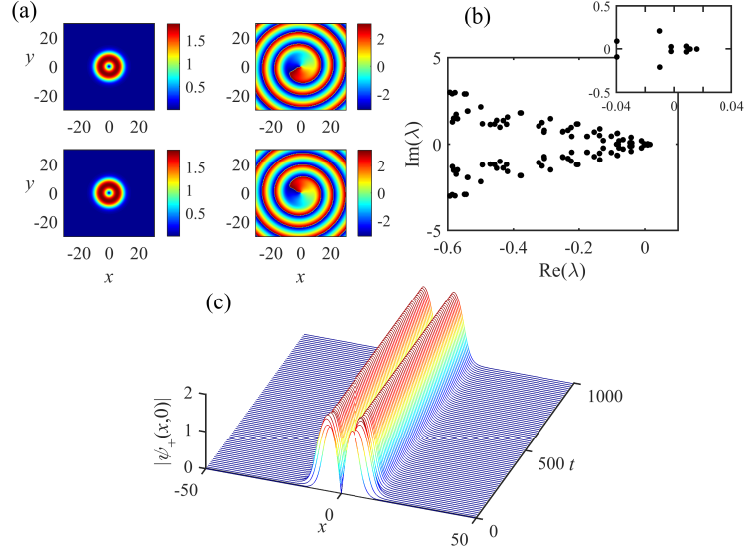


FIG. 2: The spontaneous transformation of an unstable VAV into its stable counterpart at $g = 2.07$, $\beta = 0.1$. (a) The top and bottom rows displays the amplitude and phase structure of the ψ_+ and ψ_- components, respectively, in the established stable VAV complex. (b) Some eigenvalues in the stability spectrum of the initial unstable VAV. The inset zooms the vicinity of $\lambda = 0$. (c) The spontaneous transformation, by means of the cross section of one component, $|\psi_+(x,0)|$. Both the initial unstable and final stable VAVs are designated by dots in Fig. 1, with the spontaneous transition between them schematically shown by the vertical arrows.

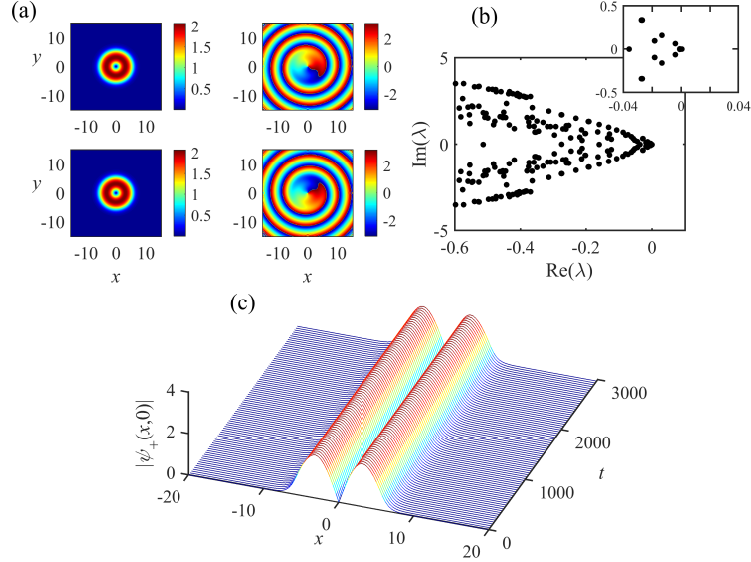


FIG. 3: (a) The top and bottom rows display the amplitude and phase structure of components ψ_+ and ψ_- , respectively, in a stable VAV mode found at $\beta = 0.8$ and $g = 2.12$, with integral power $N = 571.5$, peak density $n_{\max} = 8.53$, and positive chemical potential $\mu = 0.072$. (b) Some eigenvalues in the stability spectrum of (a). The inset zooms the vicinity of $\lambda = 0$. (c) Stability of this mode in direct simulations of its perturbed evolution.

from the above-mentioned hidden-vorticity modes, which are also built as bound states of localized components with vorticities $S = \pm 1$ in the framework of the conservative system of nonlinearly coupled GPEs, and are partly [51–53] or fully [54] unstable against the splitting instability, which breaks the respective vortex ring into fragments.

Figure 5 demonstrates that the stability window for the VAV modes remains narrow in comparison with interval (26) defined by the above-mentioned coarse necessary conditions. The window exists too at $\beta = 0$:

$$2.040 < g < 2.090, \quad (37)$$

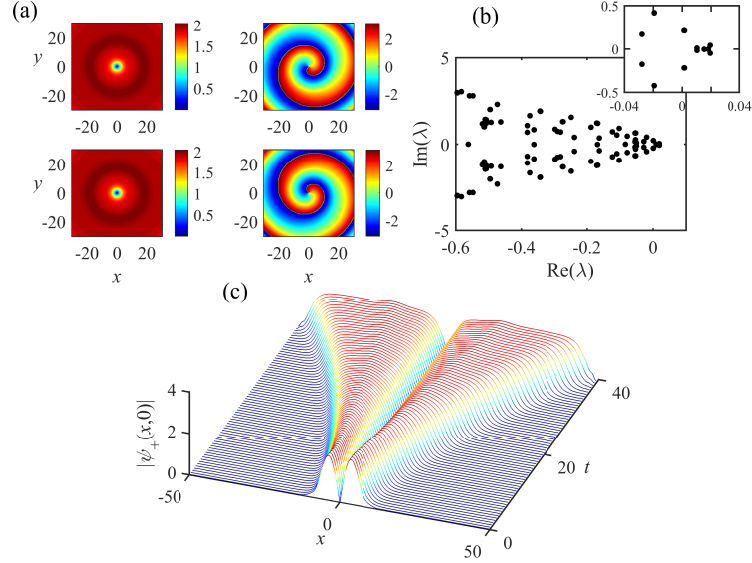


FIG. 4: The unstable VAV at $g = 2.200$, $\beta = 0.1$. (a) The top and bottom rows display the amplitude and phase structure of the ψ_+ and ψ_- components, respectively. (b) Some eigenvalues in the stability spectrum of the initial unstable VAV. The insets zoom the vicinity of $\lambda = 0$. (c) The evolution of the unstable VAV, which suffers blowup as the result of the instability development.

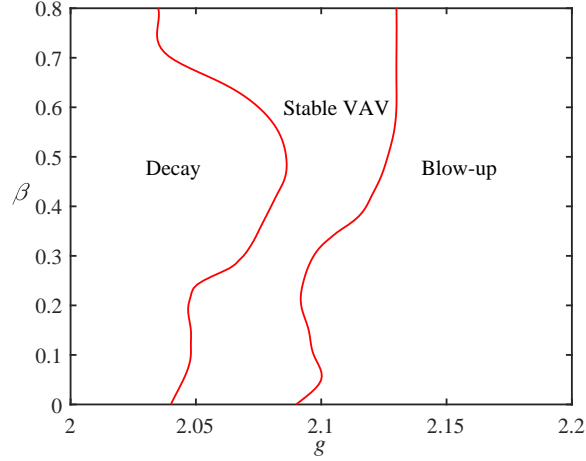


FIG. 5: The stability border for VAV modes in the plane of (g, β) for $\eta = 0$, $a = 2.0$ and $\varepsilon = 0.1$.

when SOC is absent, Eqs. (1) and (2) being coupled only by the saturable gain and loss, see Eq. (3). With the increase of the SOC coefficient up to relatively large values, $\beta \simeq 0.7$, the width of the stability region expands by a factor $\simeq 2$, still staying quite close to the center of the broad interval defined by necessary conditions (26). Systematically collected numerical data demonstrate that the same conclusions remain true at other values of parameters a and ε in the underlying model based on Eqs. (1) and (2).

B. Semi-vortex (SV) complexes, $m = 1$

Composite soliton modes corresponding to ansatz (27) with $m = 1$ were found, along with the corresponding eigenvalues μ , as stationary solutions initiated by input

$$\begin{aligned}\phi_+(x, y) &= \phi_0 \exp(-\alpha r^2), \\ \phi_-(x, y) &= (\phi_0/10) r^2 \exp(-\alpha r^2),\end{aligned}\tag{38}$$

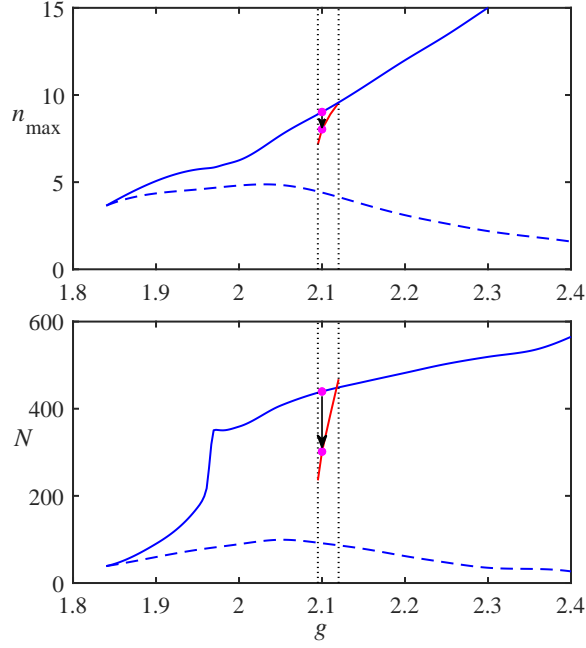


FIG. 6: The same as in Fig. 1, but for SV families, with vorticities 0 and 2 of the two components. The parameters in Eqs. (1) and (2) are the same as in Fig. 1, i.e, $\eta = 0$, $\varepsilon = 0.1$, $a = 2$, and $\beta = 0.1$. The narrow stability window (39) is exhibited by this figure. The dots connected by the vertical arrow correspond to the spontaneous transformation of an unstable SV into a stable one, as shown in Fig. 7.

Unlike input (33) which generates the VAV modes, here the amplitude of the vortex component is taken essentially smaller than in the zero-vorticity component, because the vortex component in established SV modes tends to have a relatively small amplitude [29]-[31].

The systematic numerical analysis yields a stability band for the SV modes shown in Fig. 6, which demonstrates a situation generally similar to that displayed for VAV modes in Fig. 1, but with a stability window,

$$2.095 < g < 2.120, \quad (39)$$

whose width is half of that defined by Eq. (36) for the VAVs. This interval, similar to its counterpart (36), stays close to the center of the broad interval (26), which is defined by the necessary conditions considered above.

In the present case too, three branches of stationary solutions are observed in Fig. 6, *viz.*, two unstable ones, which emerge at the bifurcation point, that virtually exactly coincides with its counterpart for the VAV states, given by Eq. (35), and a stable branch shown by the red segment in Fig. 6. Another similarity to the case of VAV modes is that, outside the stability band (39), unstable SVs decay to zero at $g < 2.095$, and undergo blowup at $g > 2.120$. On the other hand, the comparison of Figs. 1 and 6 shows that the integral power of the stable SVs is smaller than the power of the stable VAVs, roughly, by a factor of 5.

The chemical potential of the stable branch decreases nearly linearly, as a function of g , in the stability interval (36), from $\mu(g = 2.095) = 0.159$ to $\mu(g = 2.120) = 0.106$, while μ remains nearly constant in interval (39) for both unstable branches. Note that all these values of the chemical potential are positive, as they are for the VAV branches considered above.

As well as in the case of VAV modes, the stable branch is, within the limits imposed by Eq. (39), an attractor, as initial states corresponding to either of the two unstable families spontaneously transform into the stable counterpart, keeping the SV structure. A typical example of the spontaneous transformation is displayed in Fig. 7.

C. The system without the SOC terms

At $\beta = 0$, the vortex component of the SV vanishes, $\psi_- = 0$, while the zero-vorticity one turns into an axisymmetric dissipative soliton produced by the single equation (1):

$$i\partial_t\psi_+ = -(1 - i\eta)(\partial_x^2 + \partial_y^2)\psi_+ + i\left(-1 + \frac{g}{1 + \varepsilon|\psi_+|^2} - \frac{a}{1 + |\psi_+|^2}\right)\psi_+ \quad (40)$$

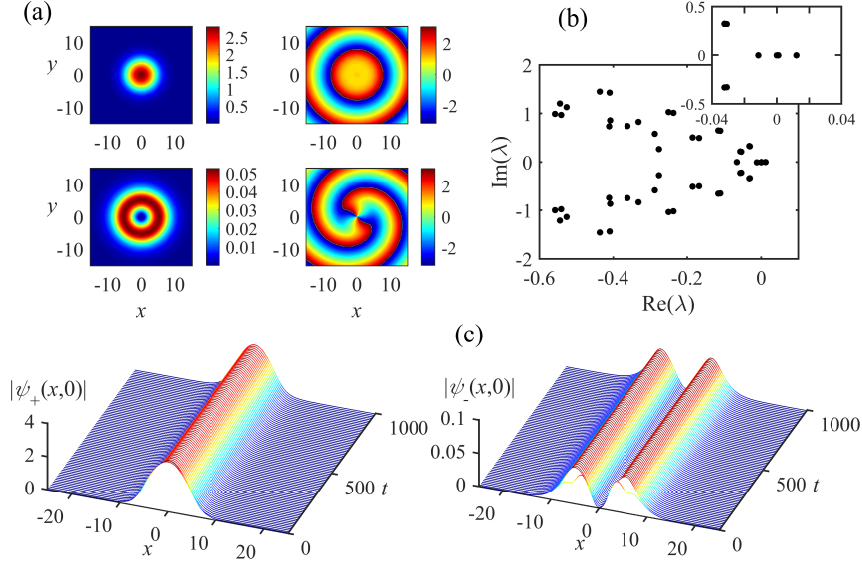


FIG. 7: (a) The top and bottom rows display the amplitude and phase structures of the zero-vorticity and vortical components (ψ_+ and ψ_- , respectively), for a stable SV mode found at $\beta = 0.1$ and $g = 2.10$, with other parameters fixed as per Eq. (4). (b) Some eigenvalues in the stability spectrum of the initial unstable SV. The insets zoom the vicinity of $\lambda = 0$. (c) The evolution of $|\psi_+(x,0)|$ and $|\psi_-(x,0)|$, which displays, at the same parameters, the spontaneous transformation of an unstable SV into the stable one. Both the initial unstable and final stable SVs are designated by dots in Fig. 6, with the spontaneous transition between them designated by the vertical arrows.

(recall we actually set $\eta = 0$). In the case of $\beta = 0$, essentially the same equation, with ψ_+ replaced by $\tilde{\psi}_+$, applies to the two-component system with equal components, of substitution $\psi_{\pm} = (1/\sqrt{2})\tilde{\psi}_+$. The numerical solution of Eq. (40) produces the respective stability window,

$$2.090 < g < 2.130, \quad (41)$$

which is somewhat broader than its counterpart (39), found for $\beta = 0.1$.

The relative narrowness of the stability windows (39) and (41) in comparison with the ones given by Eqs. (36) and (37) for VAVs suggests that SV modes are more fragile in comparison with the VAVs. This expectation is confirmed by the fact that, on the contrary to the situation for the VAVs, whose stability area tends to expand with the growth of the SOC strength β in Fig. 3, the increase of β leads to shrinkage of the SV stability window, which closes and does not exist at $\beta \geq 0.24$ (not shown here in detail). Finally, Fig. 8 summarizes the findings in the plane of (a, g) for fixed $\varepsilon = 0.1$. It is clearly seen that the region of stable zero vorticity soliton is relatively broad at large values of a . Typical example of the spontaneous transformation of unstable zero vorticity soliton is displayed in Fig. 9.

IV. CONCLUSION

The objective of this work is to construct 2D self-trapped states (dissipative solitons) in the system of CGLEs with saturable gain and absorption for SOC (spin-orbit-coupled) modes of an optical microcavity with saturable gain and loss, in the absence of any geometric trapping. The second-order linear differential operator representing SOC creates complexes with difference $\Delta S = 2$ between vorticities of the two components. Previously, 2D localized dissipative vortex states were predicted, under the action of SOC, in the presence of a trapping potential, but they were not found in the free space. Here, we have identified stable complexes of the VAV (vortex-antivortex) and SV (semi-vortex) types, i.e., ones with vorticities $(-1, +1)$ and $(0, 2)$ in the two components. The 2D solitons of the latter type are quite fragile, being stable in a very narrow (but, nevertheless, existing) window. For the VAVs, the stability interval, defined in terms of the gain coefficient, is rather narrow too, but it may be expanded by applying stronger SOC.

It is worthy to note that, on the contrary to the previously reported 2D localized states of the VAV, MM (mixed-mode), and SV types, supported by the trapping potential [41], as well as single-component trapped [50] and self-trapped [48, 49] vortices, the stability of the VAVs and SVs in the present system (including its simplified form which does not include SOC) does not require the presence of diffusion terms (dispersive linear losses, whose physical origin may be problematic) in the CGLE model. Due to the absence of the diffusion, the 2D dissipative system introduced

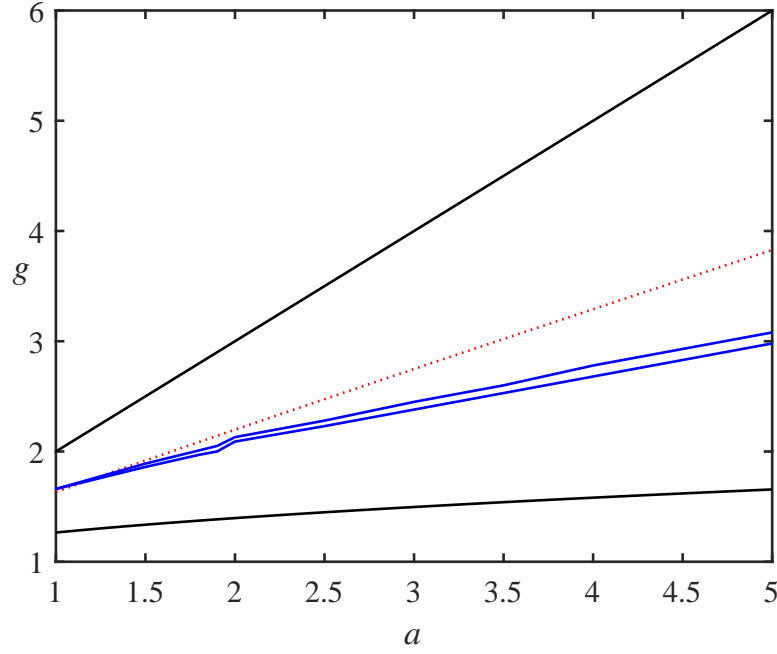


FIG. 8: The stability diagram in the plane (a, g) with $\varepsilon = 0.1$. The black solid lines are plotted by Eq. (24) while the red dotted line is the middle of the interval. The stability region for the zero vorticity soliton corresponds to the space between the blue lines. The region of the stability vanish at $a = 1$.

in this work keeps the Galilean invariance, which suggests a possibility to introduce moving solitons and simulate collisions between them (cf. Ref. [61]), as well as a possibility of forming bound states of two or several dissipative solitons. These issues should be a subject of a separate work.

Funding

Thailand Research Fund (grant BRG6080017); The Royal Society (grant IE 160465); Israel Science Foundation (grant 1286/17); ITMO University Visiting Professorship (Government of Russia Grant 074-U01).

V. REFERENCES

-
- [1] Dresselhaus 1955 *G Phys. Rev.* **100** 580
 - [2] Rashba E I and Sheka V I 1959 Symmetry of energy bands in crystals of Wurtzite type II. Symmetry of bands with spin-orbit interaction included, *Fiz. Tverd. Tela: Collected Papers* **2** 162-176 [in Russian; see English translation in: 2015 *New. J. Phys.* **17** 050202]
 - [3] Bychkov Y A and Rashba E I 1984 Oscillatory effects and the magnetic susceptibility of carriers in inversion layers *J. Phys. C* **17** 6039
 - [4] Xiao D, Chang M C, and Niu Q 2010 Berry phase effects on electronic properties *Rev. Mod. Phys.* **82** 1959-2007
 - [5] Hasan M and Kane C L 2010 Colloquium: Topological insulators, *Rev. Mod. Phys.* **82** 3045-3067
 - [6] Žutić I, Fabian J and Das Sarma S 2004 Spintronics: Fundamentals and applications, Spin-Injection spectroscopy of a spin-orbit coupled Fermi gas *Rev. Mod. Phys.* **76** 323-409
 - [7] Lin Y J, Jimenez-Garcia K, and Spielman I B 2011 Spin-orbit-coupled Bose-Einstein condensates *Nature* **471** 83-86
 - [8] Cheuk L W, Sommer A T, Hadzibabic Z, Yefsah T, Bakr W S, and Zwierlein M W 2012 *Phys. Rev. Lett.* **109** 095302
 - [9] Zhang J -Y, Ji S -C, Chen Z, Zhang L, Du Z -D, Yan B, Pan G -S, Zhao B, Deng Y J, Zhai H, Chen S, and Pan J -W 2012 Collective dipole oscillations of a spin-orbit coupled Bose-Einstein condensate, *Phys. Rev. Lett.* **109** 115301
 - [10] Dalibard J, Gerbier F, Juzeliunas G, and Öhberg P 2011 Colloquium: Artificial gauge potentials for neutral atoms, *Rev. Mod. Phys.* **83** 1523

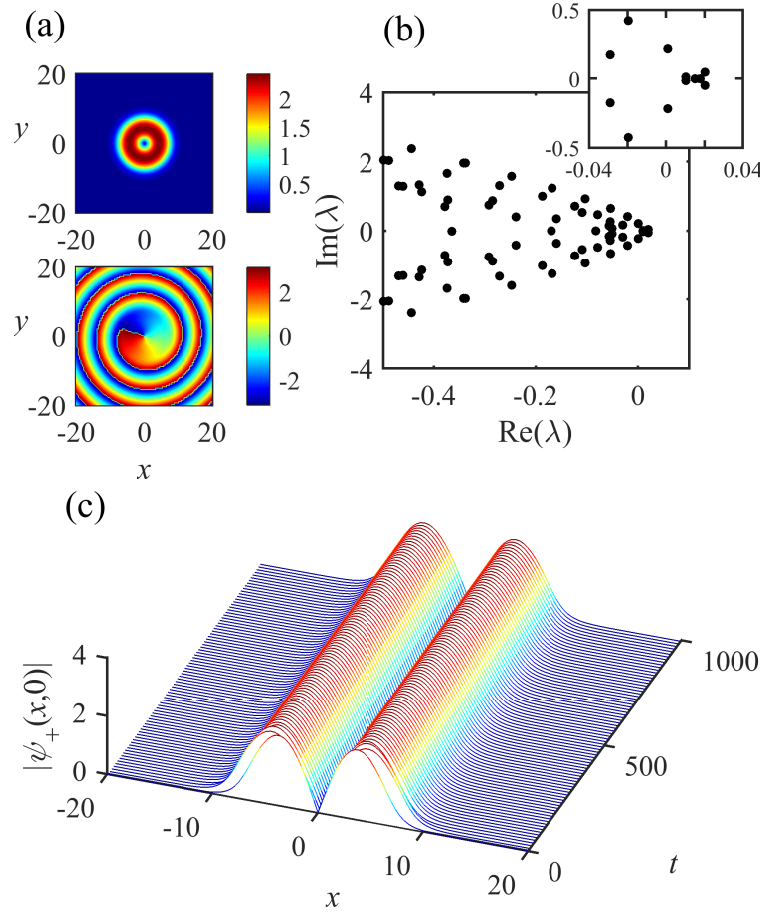


FIG. 9: An example of the zero vorticity soliton for $g = 2.75$ and $a = 4.0$. (a) The amplitude and phase of ψ_+ component (at $t = 1000$). (b) Some eigenvalues in the stability spectrum of the initial unstable zero vorticity. The insets zoom the vicinity of $\lambda = 0$. (c) The evolution of $|\psi_+(x,0)|$ showing the spontaneous transformation of unstable zero vorticity soliton into a stable one.

- [11] Galitski V and Spielman I B 2013 Spin-orbit coupling in quantum gases *Nature* **494**, 49-54
- [12] H. Zhai, Degenerate quantum gases with spin-orbit coupling: a review, *Rep. Prog. Phys.* **78**, 026001 (2015).
- [13] Schulz S, Schumacher S, and Czycholl G, (2008) Spin-orbit coupling and crystal-field splitting in the electronic and optical properties of nitride quantum dots with a wurtzite crystal structure, *Eur. Phys. J. B* **64** 51-60.
- [14] Shelykh I A, Kavokin A V, Rubo Y G, Liew T C W, and Malpuech G 2010 Polariton polarization-sensitive phenomena in planar semiconductor microcavities *Semicond. Sci. Technol.* **25** 013001
- [15] Sala V G, Solnyshkov D D, Carusotto I, Jacqmin T, Lemaître I, Terças H, Nalitov A, Abbarchi M, Galopin E, Sagnes I, Bloch J, Malpuech G, and Amo A 2015 Spin-Orbit coupling for photons and polaritons in microstructures *Phys. Rev. X* **5** 011034
- [16] S. Dufferwiel, F. Li, E. Cancellieri, L. Giriunas, A. A. P. Trichet, D. M. Whittaker, P. M. Walker, F. Fras, E. Clarke, J. M. Smith, M. S. Skolnick, and D. N. Krizhanovskii, Spin textures of exciton-polaritons in a tunable microcavity with large TE-TM splitting, *Phys. Rev. Lett.* **115** 246401 (2015).
- [17] Lafont O, Luk S M H, Lewandowski P, Kwong N H, Leung P T, Galopin E, Lemaître A, Tignon J, Schumacher S, Baudin E, and Binder R 2017 Controlling the optical spin Hall effect with light *Appl. Phys. Lett.* **110** 061108
- [18] Bliokh K Y, Rodriguez-Fortuno F J, Nori F, and Zayats A V 2015 Spin-orbit interactions of light, *Nature Phot.* **9** 796-808
- [19] Flayac H, Shelykh I A, Solnyshkov D D, and Malpuech G 2010 Topological stability of the half-vortices in spinor exciton-polariton condensates *Phys. Rev. B* **81** 045318
- [20] Selmi F, Coulibaly S, Loghmari Z, Sagnes I, Beaudoin G, Clerc M G, and Barbay S 2016 Spatiotemporal Chaos Induces Extreme Events in an Extended Microcavity Laser *Phys. Rev. Lett.* **116** 013901
- [21] Jimenez-Garcia J, Rodriguez P, Guillet T, and Ackemann T 2017 Spontaneous Formation of Vector Vortex Beams in Vertical-Cavity Surface-Emitting Lasers with Feedback *Phys. Rev. Lett.* **119** 113902
- [22] Marconi M, Javaloyes J, Barland S, Balle S, and Giudici M 2015 Vectorial dissipative solitons in vertical-cavity surface-emitting lasers with delays *Nature Phot.* **9** 450-455

- [23] Gustave F, Radwell N, McIntyre C, Toomey J P, Kane D M, Barland S, Firth W J, Oppo G -L , and Ackemann T 2017 Observation of mode-locked spatial laser solitons *Phys. Rev. Lett.* **118** 044102
- [24] Averlant E, Tlidi M, Thienpont H, Ackemann T, and Panajotov K 2016 Vector cavity solitons in broad area vertical-cavity surface-emitting lasers *Sci. Rep.* **6** 20428
- [25] Turconi M, Prati F, Barland S, and Tissoni G 2015 Excitable solitons in a semiconductor laser with a saturable absorber *Phys. Rev. A* **92** 053855
- [26] Elsass T, Gauthron K, Beaudoin G, Sagnes I, Kuszelewicz R, and Barbay S 2010 Control of cavity solitons and dynamical states in a monolithic vertical cavity laser with saturable absorber *The European Physical Journal D* **59** 91-96
- [27] Genevet P, Barland S, Giudici M, Tredicce J R 2010 Bistable and Addressable Localized Vortices in Semiconductor Lasers *Phys. Rev. Lett.* **104** 223902
- [28] Ramachandran B, Opanchuk B, Liu X-J , Pu H, Drummond P D, and Hu H 2012 *Phys. Rev. A* **85** 023606
- [29] Sakaguchi H, Li B, and Malomed B A 2014 Creation of two-dimensional composite solitons in spin-orbit-coupled self-attractive Bose-Einstein condensates in free space, *Phys. Rev. E* **89** 032920
- [30] Sakaguchi H, Sherman E Ya, and Malomed B A 2016 Vortex solitons in two-dimensional spin-orbit coupled Bose-Einstein condensates: Effects of the Rashba-Dresselhaus coupling and the Zeeman splitting, *Phys. Rev. E* **94** 032202
- [31] Sakaguchi H, Li B., Sherman E Ya, and Malomed B A 2018 Composite solitons in two-dimensional spin-orbit coupled self-attractive Bose-Einstein condensates in free space *Romanian Reports in Physics* **70** 502
- [32] Chiao R Y, Garmire E and Townes C H 1964 Self-trapping of optical beams *Phys. Rev. Lett.* **13** 479
- [33] Yankauskas Z K 1966 Radial field distributions in a self-focusing beam *Sov. Radiophysics* **9** 261-263
- [34] Kruglov V I and Vlasov R A 1985 Spiral self-trapping propagation of optical beams in media with cubic nonlinearity *Phys. Lett. A* **111** 401-404
- [35] Kruglov V I, Logvin Y V, and Volkov V M 1992 The theory of spiral laser beams in nonlinear media *J. Mod. Opt.* **39** 2277-2291
- [36] Skryabin D V 2001 Instabilities of vortices in a binary mixture of trapped Bose-Einstein condensates: Role of collective excitations with positive and negative energies *Phys. Rev. A* **63** 013602
- [37] Bergé L 1998 Wave collapse in physics: principles and applications to light and plasma waves *Phys. Rep.* **303** 259-370
- [38] Fibich G 2015 *The Nonlinear Schrödinger Equation: Singular Solutions and Optical Collapse* (Springer, Heidelberg).
- [39] Firth W J and Skryabin D V 1997 Optical solitons carrying orbital angular momentum *Phys. Rev. Lett.* **79** 2450
- [40] Skryabin D V and Firth W J 1998 Dynamics of self-trapped beams with phase dislocation in saturable Kerr and quadratic nonlinear media *Phys. Rev. E* **58** 3916
- [41] Sakaguchi H, Malomed B A, and Skryabin D V 2017 Spin-orbit coupling and nonlinear modes of the polariton condensate in a harmonic trap *New J. Phys.* **19** 08503
- [42] Borgh M O, Keeling J, and Berloff N G 2010 Spatial pattern formation and polarization dynamics of a nonequilibrium spinor polariton condensate *Phys. Rev. B* **81** 235302
- [43] Schneider C, Winkler K, Fraser M D, Kamp M, Yamamoto Y, Ostrovskaya E A, and Höfling S 2017 Exciton-polariton trapping and potential landscape engineering *Rep. Prog. Phys.* **80** 016503
- [44] Vladimirov A G, Fedorov S V, Kaliteevskii N A, Khodova G V, and Rosanov N N 1999 Numerical investigation of laser localized structures *J. Opt. B: Quantum Semiclass. Opt.* **1** 101-106
- [45] Fedorov S V, Vladimirov A G, Khodova G V, and Rosanov N N 2000 Effect of frequency detunings and finite relaxation rates on laser localized structures *Phys. Rev. E* **61** 5814-5824
- [46] Veretenov N A, Fedorov S V, Rosanov N N 2017 Topological Vortex and Knotted Dissipative Optical 3D Solitons Generated by 2D Vortex Solitons *Phys. Rev. Lett.* **119** 263901
- [47] Marini A and Skryabin D V 2010 Ginzburg-Landau equation bound to the metal-dielectric interface and transverse nonlinear optics with amplified plasmon polaritons *Phys. Rev. A* **81** 033850
- [48] Crasovan L -C , Malomed B A, and Mihalache D 2001 Stable vortex solitons in the two-dimensional Ginzburg-Landau equation *Phys. Rev. E* **63** 016605
- [49] Mihalache D, Mazilu D, Lederer F, Leblond H, and Malomed B A 2007 Stability limits for three-dimensional vortex solitons in the Ginzburg-Landau equation with the cubic-quintic nonlinearity *Phys. Rev. A* **76** 045803
- [50] Maytevarunyoo T, Malomed B A, and Skryabin D V 2018 One- and two-dimensional modes in the complex Ginzburg-Landau equation with a trapping potential *Opt. Exp.* **26** 8849-8865
- [51] Brtko M, Gammal A, and Malomed B A 2010 Hidden vorticity in binary Bose-Einstein condensates *Phys. Rev. A* **82** 053610
- [52] Ma X K, Driben R, Malomed B A, Meier T, and Schumacher S 2016 Two-dimensional symbiotic solitons and vortices in binary condensates with attractive cross-species interaction *Sci. Rep.* **6** 34847
- [53] Li Y, Chen Z, Luo Z, Huang C, Tan H, Pang W, and Malomed B A 2018 Two-dimensional vortex quantum droplets arXiv:1801.10274
- [54] Kartashov Y V, Malomed B A, Tarruell L, and Torner L 2018 Three-dimensional droplets of swirling superfluids *Phys. Rev. A* **98** 013612
- [55] Musslimani Z H, Segev M, and Christodoulides D N 2000 Multicomponent two-dimensional solitons carrying topological charges *Opt. Lett.* **25** 61-63
- [56] Musslimani Z H, Segev M, Christodoulides D N, and Soljačić M 2000 Composite multihump vector solitons carrying topological charge *Phys. Rev. Lett.* **84** 1164-1167
- [57] Pereira N R and Stenflo L 1977 Nonlinear Schrödinger equation including growth and damping *Phys. Fluids* **20** 1733-1734
- [58] Malomed B A 1987 Evolution of nonsoliton and “quasiclassical” wavetrains in nonlinear Schrödinger and Korteweg - de

- Vries equations with dissipative perturbations *Physica D* **29** 155-172
- [59] Aranson I S and Kramer L 2002 The world of the complex Ginzburg-Landau equation *Rev. Mod. Phys.* **74** 99-143
- [60] Yang J 2010 *Nonlinear Waves in Integrable and Nonintegrable Systems* (SIAM: Philadelphia).
- [61] Sakaguchi H 2005 Motion of pulses and vortices in the cubic-quintic complex Ginzburg-Landau equation without viscosity *Physica D* **210** 138-148